Vertically emitting indium phosphide nanowire lasers

Wei-Zong Xu[1,2,4†], Fang-Fang Ren[1,2,4†*], Dimitars Jevtics[3], Antonio Hurtado[3*], Li Li[1], Qian Gao[1], Jiandong Ye[1,2], Fan Wang[1,5], Benoit Guilhabert[3], Lan Fu[1], Hai Lu[2,4], Rong Zhang[2,4], Hark Hoe Tan[1], Martin D. Dawson[3], and Chennupati Jagadish[1]

[1] *Department of Electronic Materials Engineering, Research School of Physics and Engineering, The Australian National University, Canberra, ACT 2601, Australia*

[2] *School of Electronic Science and Engineering, Nanjing University, Nanjing 210093, China*

[3] *Institute of Photonics, SUPA Department of Physics, University of Strathclyde, Technology and Innovation Centre, 99 George Street, G1 1RD Glasgow, U.K.*

[4] *Collaborative Innovation Center of Advanced Microstructures, Nanjing University, Nanjing 210093, China*

[5] *Institute for Biomedical Materials and Devices (IBMD), Faculty of Science, University of Technology Sydney, NSW 2007, Australia*

Abstract: Semiconductor nanowire (NW) lasers have attracted considerable research effort given their excellent promise for nanoscale photonic sources. However, NW lasers currently exhibit poor directionality and high threshold gain, issues critically limiting their prospects for on-chip light sources with extremely reduced footprint and efficient power consumption. Here, we propose a new design and experimentally demonstrate a vertically emitting indium phosphide (InP) NW laser structure showing high emission directionality and reduced energy requirements for operation. The structure of the laser combines an InP NW integrated in a cat's eye (CE) antenna. Thanks to the antenna guidance with broken asymmetry, strong focusing ability and high-*Q* factor, the designed InP CE-NW lasers exhibit a higher degree of polarization, narrower emission angle, enhanced internal quantum efficiency and reduced lasing threshold. Hence, this NW laser-antenna system provides a very promising approach towards the achievement of

[†]These authors contributed equally to this work. [*]e-mail: ffren@nju.edu.cn; antonio.hurtado@strath.ac.uk

high-performance nanoscale lasers, with excellent prospects for use as highly localized light sources in present and future integrated nanophotonics systems for applications in advanced sensing, high-resolution imaging and quantum communications.

Keywords: Nanowire lasers, vertical emission, plasmonic antennas, photonic integration

Semiconductor nanowires (NWs) have emerged as potential building blocks in advanced optical and nanophotonic devices and compact integrated circuits given their ultra-small dimensions and remarkable performance [1-6]. To date, intensive research has been conducted on the use of semiconducting NWs as gain media for smaller and faster lasers, critically important aspects for optical data transmission, sensing and imaging applications [7-10]. In order to demonstrate lasing from semiconductor NWs, these have usually been transferred from their growth substrate onto another secondary surface to ensure a large refractive index contrast between the NWs and their surrounding media [3,8]. Above lasing threshold, characteristic interference fringes can be observed from the NW lasers, similar to interference patterns generated by two coherent dipole emitters separated by the NW's length [3], indicative of spatially coherent light emission from the NW's end facets. However, in spite of the high promise of these nanoscale lasers for breakthroughs in nanophotonics, their light emission has a poor directionality with a diffracted beam resulting from the sub-wavelength size of NWs [11-14]. This leads to high coupling losses between NW lasers and optical fibers or waveguides. It currently limits their integration into three-dimensional on-chip devices, which indeed requires a small vertical divergence of the emission angle.

On the other hand, enhancing the emission intensity of NW lasers whilst simultaneously miniaturizing their footprint remains a challenging issue. There are minimum diameter and length requirements for NWs to support lasing action at threshold powers below the thermal vaporization limit of the semiconducting material [3]. Moreover, the directionality of NW lasers worsens as their size reduces. Therefore, the peripheral antenna design proposed in this work becomes an efficient solution to enhance their quantum efficiency. Additionally, to further downscale the physical device size beyond the diffraction limit, plasmonic lasers have been recently proposed [10,14-18] relying on NWs (functioning as gain medium) coupled to external metallic plasmonic structures. The latter allow storage of most of the energy in surface plasmons with a coherent excitation of the electrons on the metallic surface. As a result, lasing operation can be obtained with reduced optical mode volume below the diffraction limit [10,14-15,17-19]. However, the threshold powers in plasmonic nanolasers are much larger than in their photonic counterparts, given

the high propagation losses in metals [14-17]. Therefore, the development of efficient nanolasers with ideal directionality, reduced foot-print and low-threshold remains a fundamental challenge.

This work focuses on these challenges, proposing and demonstrating a vertically emitting InP NW laser with low lasing threshold, high directionality and reduced foot-print. This is based on a rational design combining an aluminum (*Al*) cat's eye (CE) antenna (also known as split bull's eye antenna [20]) with an InP NW, simultaneously allowing tailoring of its emission profile and efficiency. InP NWs have already proven to be attractive candidates for compact light sources in miniaturized optical applications [8,21], whilst CE antennas have shown excellent performance in near- and mid-infrared photodetectors with high concentration ability and sensitive polarization dependence [20,22-23]. Additionally, the focusing ability [24,25], high reflectivity, coupling capability of surface plasmons, and symmetry breaking of the CE antenna also reveals its lens-like properties and beaming effect of the NW far-field emission. Hence, the proposed design merging an InP NW with an *Al* CE antenna offers a tailored emission profile and enhanced efficiency enabling the fabrication of vertically emitting InP NW lasers with performance unseen to date including higher degree of polarization, greatly improved emission directionality and ultra-low lasing threshold power requirements.

Figure 1a shows the structure of the proposed InP NW CE laser (Sample A) comprising an ultra-small InP NW integrated with an *Al* CE antenna on a quartz substrate. The NW's geometry, i.e. diameter w = 290 nm and length L = 900 nm (Figure 1b), has been optimized to support the TE_{11} and TE_{01} guided optical modes at the wavelengths of ~750 and 870 nm, these being the near-band emissions of InP NWs at cryogenic (~7 K) and room temperature (RT), respectively (see Supporting Information, Figure S1). Here, the TE and TM modes correspond to the excitation cases with light polarized along E_x and E_y respectively. It should be noted that the required minimum threshold gain for an InP NW with w = 290 nm and L = 900 nm is calculated to be 2400 cm^{-1} (see Supporting Information, Figure S4). This high level indicates that no lasing action would be obtained from a bare InP NW (Sample B) below the material thermal vaporization limit.

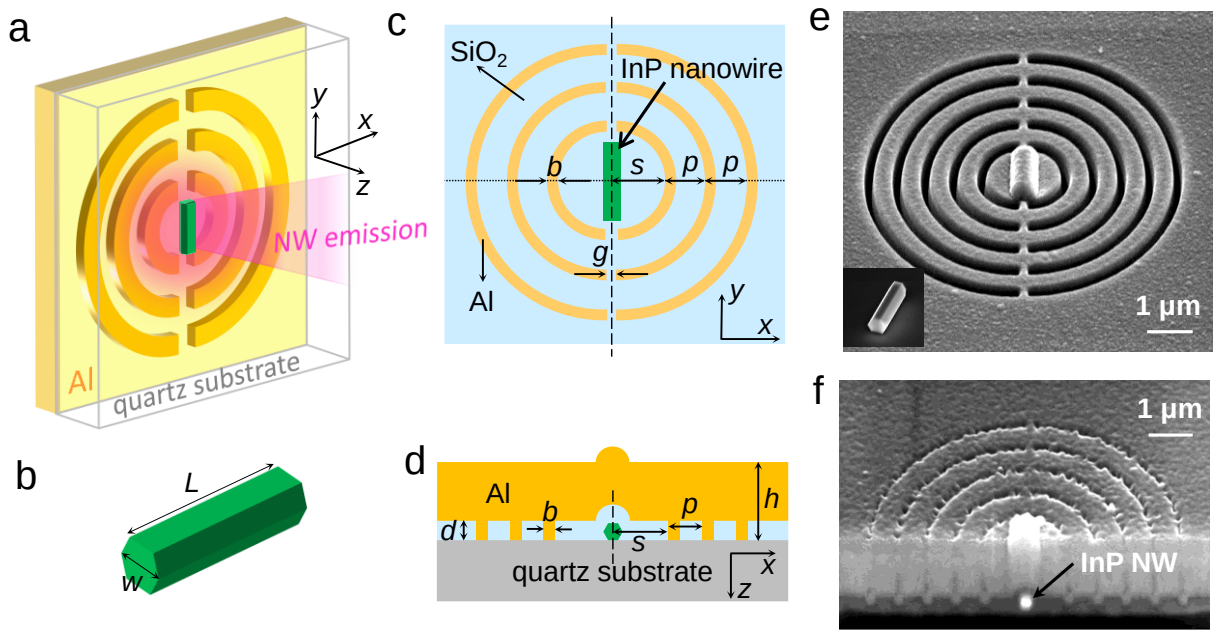

Figure 1. Structure of the vertically emitting InP NW CE laser (Sample A). (a) Full device layout showing the CE laser structure consisting of a single InP NW embedded in the CE antenna. (b) Geometry of the InP NW. (c,d) Top-view and cross-section schematics of the CE laser showing the various dimensions. (e) Oblique SEM image of the CE laser before *Al* deposition. Inset: SEM image of an InP NW (w = 290 nm and L= 900 nm) transferred onto a quartz substrate. (f) Oblique SEM image of the cross-section of the fabricated device after *Al* deposition.

The design of the CE antenna was divided into two steps. First, the inner circular grating, located at a distance s from the antenna's center (Figure 1c,d), was designed to form an enhanced Q-factor metal resonant cavity for the NW's guided modes. The calculated intensity spectra for both TE and TM modes are given in the Supporting Information (Figure S2a,b). Under E_x incidence (i.e. TE mode), due to Fabry-Perot resonances the intensity reaches a maximum at λ = 870 nm when $s \approx$ 650, 900, 1200, 1500 nm, etc. Also, since the Q-factor compares the cavity's gain and loss ratio, a higher Q-factor indicates lower lasing threshold requirements. Here, $s \approx$ 900 nm was chosen to ensure a higher Q-factor compared to that obtained for an infinite value of s (see Supporting Information, Figure S2c). Additionally, this distance allowed the creation of a gap between the NW and CE antenna, needed to avoid etching damage on the InP NW during the focused ion beam (FIB) fabrication process. The second step was to optimize the periodical circular grating to create surface corrugations surrounding the NW to guarantee efficient surface

plasmon (SP) coupling at λ = 870 nm. A 300-nm thick SiO_2 low-index cladding layer was deposited on top of the NW to ensure high refractive index contrast between the NW and its surrounding medium. This SiO_2 cladding layer was taken into account in the *Q*-factor calculations and in the momentum conservation law for SP-grating coupling [20]. Based on simulations carried out with the commercial software tool FDTD Solutions (Lumerical Corp.), the optimal design parameters were: grating period, p = 650 nm, metallic concentric grating width b = 200 nm and depth d = 300 nm, split-gap width g = 200 nm, and inner circular grating distance, s = 900 nm, considering both the SP excitation and maximum far-field beaming effect (see Supporting Information, Part I). We also fabricated two additional reference Samples B and C. Sample B consisted of an InP NW laying horizontally on a bare quartz substrate, whilst Sample C was formed by an InP NW coated with a 1 μm-thick *Al* film on a 300-nm thick un-patterned SiO_2 cladding layer. Due to the strong *Al* reflection in Samples A and C, the optical measurements for these two samples were performed using back illumination and light collection. Alternatively, Sample B was characterized using a typical front-illumination configuration.

The fabrication procedures of the InP NW CE lasers and reference samples and the growth details of the InP NWs, are described in the Methods section. Positioning ultra-small NWs (w = 290 nm, L = 900 nm) on the center of a CE antenna with controlled orientation is a difficult task. To overcome this issue, we developed an *in-situ* fabrication procedure with excellent alignment and repeatability based on device growth and etching techniques. Figure 1e shows a scanning electron microscopy (SEM) image of the fabricated concentric grating pattern on a 300 nm-thick dielectric SiO_2 layer with an integrated InP NW underneath. The inset shows the top view of an InP NW transferred onto a quartz substrate before the deposition of SiO_2. The *Al* antenna was fabricated by FIB and selective etching processes (see SEM image in Figure 1f). It is worth noting that the surrounding metal structure provides extra confinement for the hybrid optical modes guided in the NW due to the improved overlap between optical field distribution and gain medium (InP) which enhances the internal quantum efficiency considerably. This fabrication process permitted lasing to be successfully achieved (at ~7 K) from Sample A with ultra-small size.

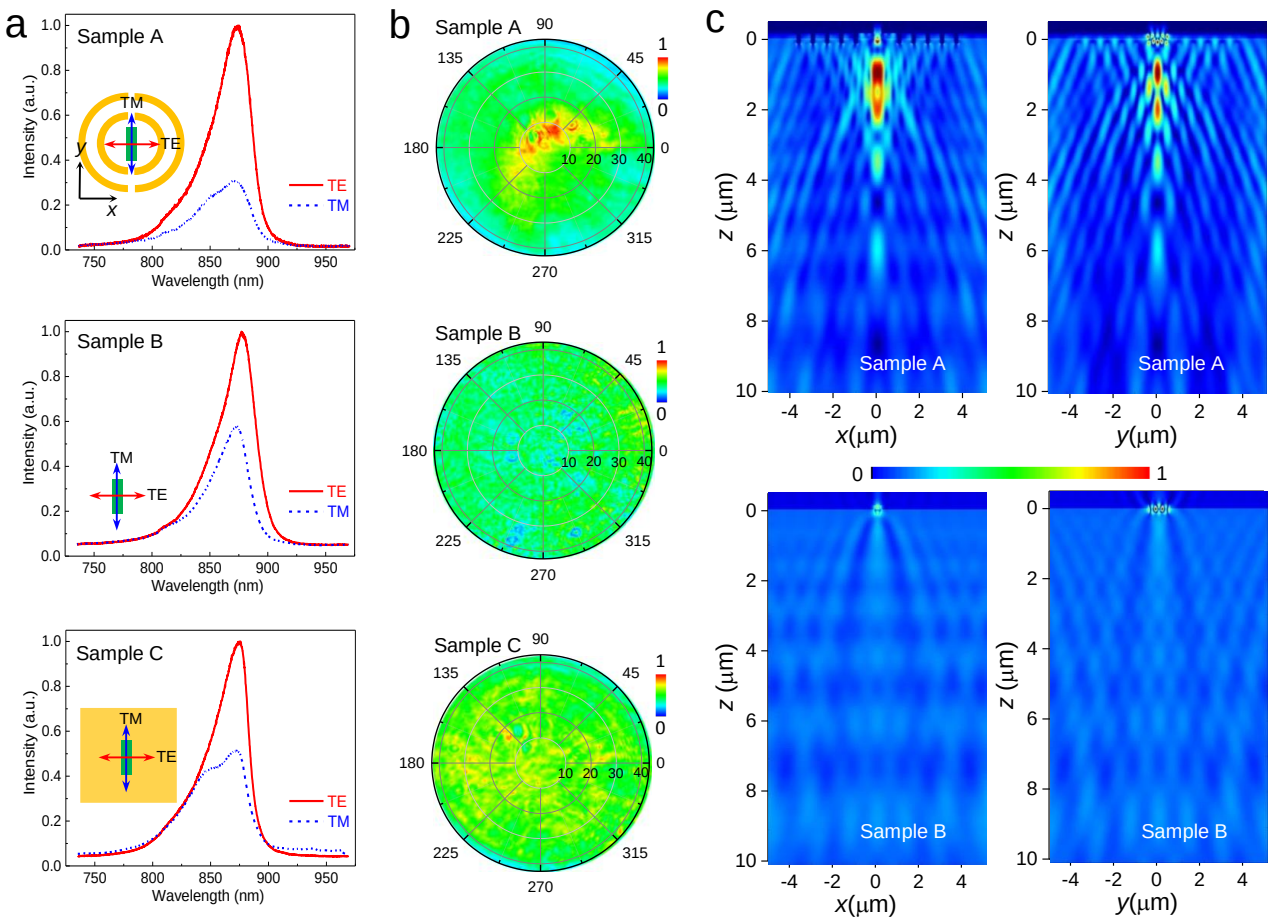

Figure 2. Polarization dependence and directionality characterization of light emission from Samples A-C. (a) Measured TE and TM polarization light emission spectra from Samples A-C where the NW geometry is shown inset. (b) Emitted light angular distribution profiles of Samples A-C used to investigate their far-field emission characteristics. A pumping fluence of 0.8 mJ/cm^2 per pulse was used at RT. (c) Simulated electric field distribution along the propagating direction on both *x*-*z* and *y*-*z* planes for Samples A and B. The colour bar shows normalized intensity (dark blue = 0, red = 1).

Complementarily, we also demonstrate room-temperature (RT) lasing emission from InP NW CE lasers, fabricated using InP NWs with larger dimensions by means of a newly developed hybrid nanofabrication technique. The latter is referred to as nanoscale transfer printing (nano-TP) [26,27] and utilizes the adhesive properties of elastomeric stamps to enable the simple, precise, and efficient positioning of semiconductor NWs at targeted locations onto diverse substrates. Using this simple hybrid approach we produced InP NW CE structures (Samples D and E) by integrating InP NWs (w = 435 nm, L = 5 μm) onto pre-fabricated CE antennas, lasing at RT at λ ~860 nm. Larger NWs with lower RT threshold

gain for lasing were used here, as compared to those utilized in Samples A-C for low temperature analysis.

Controllable light emission directionality and polarization are highly desirable features for future on-chip light sources. Hence, we have focused on investigating these important aspects. Figure 2a illustrates the polarization characteristics of our InP NW CE structure. As numerically predicted (see Supporting Information, Figure S2), the InP NW emission under excitation with light polarized along E_x (TE mode) can be significantly improved by the *Al* antenna (when compared to the TM mode). This results in an enhanced degree of polarization (DOP) of 0.7 at the wavelength of 870 nm for an InP NW with a CE antenna (Sample A, Figure 2a), where DOP = $(I_x\text{-}I_y)/(I_x+I_y)$ [28-29]. This is higher than the DOP of 0.5 obtained for a bare NW (Sample B, Figure 2a). To exclude the possibility this DOP enhancement in Sample A arises from reflections at the *Al* layer, we have also measured the polarization-dependent emission spectrum from a device with an *Al* layer but without the concentric grating pattern (Sample C). Figure 2a shows that no distinct DOP enhancement can be observed for sample C as compared to sample B. We therefore conclude that the improved DOP of Sample A is a direct result of the polarization sensitivity of the integrated split-gap CE antenna.

We have also analyzed the light emission directionality of the InP NW CE structure. This was characterized using far-field imaging to examine the angular distribution of the emitted light when a pumping fluence of 0.8 mJ/cm^2 was utilized at RT (see Figure 2b). Comparing the results obtained from Samples B and C, Figure 2b shows that the emission intensity is considerably enhanced in Sample C due to the addition of the *Al* coating reflection. However, the directionality still remains poor for Samples B and C. Significantly, a much better vertical light emission directionality is observed from the InP NW CE structure (Sample A), together with a higher emission intensity. Similar features were observed in the angle-resolved far-field lasing radiation patterns (see Supporting Information, Figure S7) thus clearly indicating that the integrated CE nanoantenna strongly governs the propagation direction of the NW's emission. To better illustrate the physical mechanism of the CE nanoantenna light-focusing functionality, we calculated the electric field distribution in the *x*-*z* and *y*-*z* planes for Samples A and B (see Figure 2c).

Two distinct features are observed for Sample A: (i) coherent interference is obtained with a focusing spot at z = 1 μm, as the phase distribution has a parabolic curve below the *Al* grating, which enables the CE structure to act as a near-field focusing lens to concentrate more emission in the vertical direction and consequently an excellent far-field directionality (see Supporting Information, Figure S8); (ii) highly localized emission can also be found inside the NW, as a result of the enhanced *Q*-factor due to the combination of the NW cavity and the inner circular grating.

Lasing characterization measurements were performed on Samples A (InP NW CE laser) and B (bare NW) using a micro-photoluminescence (micro-PL) setup. The samples were optically pumped using a pulsed laser (λ = 522 nm) at low-temperature (LT, ~7 K). Figure 3a shows the micro-PL spectra obtained from Samples A and B under different pumping fluences from 1.0 to 18.0 mJ/cm^2. At low pumping fluences, a single broad peak around 840 nm appears in both samples. With increasing fluence up to 18.0 mJ/cm^2 (limit of our micro-PL system), the luminescent intensity increases almost linearly but lasing is not observed for the bare InP NW (Sample B). On the other hand, for Sample A, upon exceeding a lasing threshold of only 5.8 mJ/cm^2, an additional peak emerges at λ = 775 nm showing a dramatic increase of output intensity and a sudden linewidth narrowing. The observed spectral clamping indicates transition from spontaneous (spectrally broad emission) to amplified spontaneous emission (multiple peaks in the envelope of the broad emission spectrum) and finally reaching lasing (single narrow peak). Figure 3b plots the LT lasing output intensity versus pumping fluence. The standard "S" shape behavior on the log-log scale can be observed for Sample A, together with a sharp cutoff of the peak's full width half maximum (FWHM) at threshold (inset in Figure 3b). All these features verified the occurrence of low-threshold lasing in the InP NW CE structure. Additionally, RT time-resolved PL measurements (see Figure 3c), revealed a carrier lifetime for Sample A of 540 ps, shorter than the 760 ps for Sample B. The lifetime reduction is mainly attributed to the combination of high cavity quality (i.e. high *Q*-factor) and strong confinement, which enhances light-matter interaction and increases the radiative spontaneous emission rate in terms of the Purcell effect. The RT internal quantum efficiency (IQE) (in Figure 3d) were measured

and extracted from the variation in the integrated PL intensity as a function of excitation power density and based on rate-equations analyses following the approach described in [30]. Clear improvement in IQE has been obtained from Sample A (with the CE antenna), as compared to Samples B and C, which further verifies the distinct localization of optical energy densities in the NW cavity. The error bars in Figure 3d indicate the variation in IQE arising from measurements on at least five different samples under the same experimental conditions.

As discussed in Supporting Information (Section IV), the achievement of room-temperature (RT) lasing requires the use of larger NWs exhibiting lower lasing thresholds. For ease of fabrication, we employed a hybrid nanoscale Transfer Printing (nano-TP) fabrication technique [26,27] to integrate larger-sized InP NWs onto pre-fabricated *Al* CE nanoantennas (as described in the Methods section). The inset in Figure 4a shows an SEM image of the InP NW CE laser (Sample D) fabricated by heterogeneously integrating an InP NW (w = 435 nm, L = 5 μm) using nano-TP onto a CE nanoantenna with the following structural parameters: p = 900 nm, b = 650 nm, d = 200 nm, g = 600 nm and s = 600 nm. We should note that the SEM image in Figure 4a reveals the presence of another smaller InP NW in the CE antenna (in its outer ring), accidentally located there but which does not affect the lasing properties of the primary larger NW. We also characterized the RT light emission from this hybrid InP NW CE laser using the micro-PL setup described in [26,27] where optical pumping was carried out with a (λ = 532 nm) pulsed laser (1.6 ns long pulses at 10 kHz repetition rate). Figure 4a plots the threshold curve of Sample D, showing the onset of RT lasing at a low pumping fluence of ~ 2 mJ/cm^2. Figure 4b shows the achievement of narrow spectral emission at RT when the device is pumped with a fluence of 4.68 mJ/cm^2. The inset in Figure 4b shows a micrograph of the lasing emission from Sample D at that fluence. Moreover, to clearly demonstrate the contribution of the CE nanoantenna, we have also fabricated for comparison purposes Sample E, formed simply by a bare InP NW laser (w = 435 nm, L = 5 μm) placed on an SiO_2 substrate. Figure 4c shows the RT threshold curve of Sample E which has a higher lasing threshold (~10 mJ/cm^2), while Figure 4d shows its lasing spectrum and a micrograph of the NW at a fluence of 32.01 mJ/cm^2. The higher lasing threshold

for Sample E under similar pumping conditions clearly demonstrates the contribution of the integrated CE nanoantenna in reducing the lasing threshold for the InP NW. Additionally, a further comparison between the lasing thresholds achieved in an InP NW CE laser and a bare NW laser onto a planar Al surface, also showing reduced lasing threshold achievement for the coupled nanowire-nanoantenna laser system is included in the Supporting Information (Section VI).

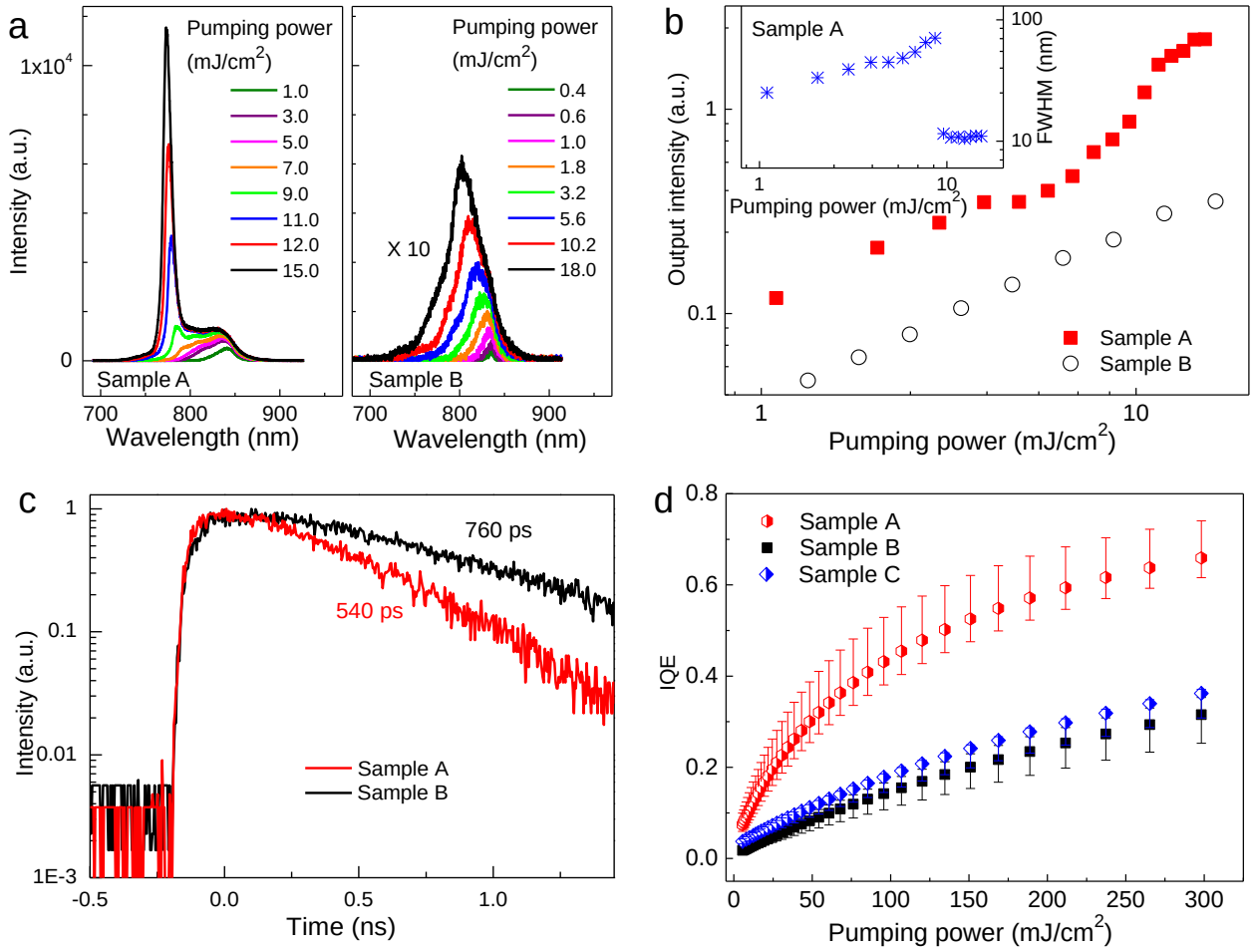

Figure 3. Lasing characterization from nanowire Samples A-C. (a) LT PL spectra at different pumping powers from Samples A and B. (b) Emission intensity as a function of pump fluence from Samples A (red solid squares) and B (black open circles) at LT. An "S" type behavior on the log-log scale can be observed in Sample A. The inset shows the evolution of the FWHM of the emission spectrum as a function of pumping power. (c) RT time-resolved spontaneous emission under weak pumping conditions. A reduction in lifetime for Sample A is observed as compared to Sample B. (d) Statistical results of IQE as a function of pumping power for Samples A (red), B (black) and C (blue) at RT. The data points were estimated by fitting the variation in integrated PL intensity as a function of excitation power density using the rate-equations model in ref [30].

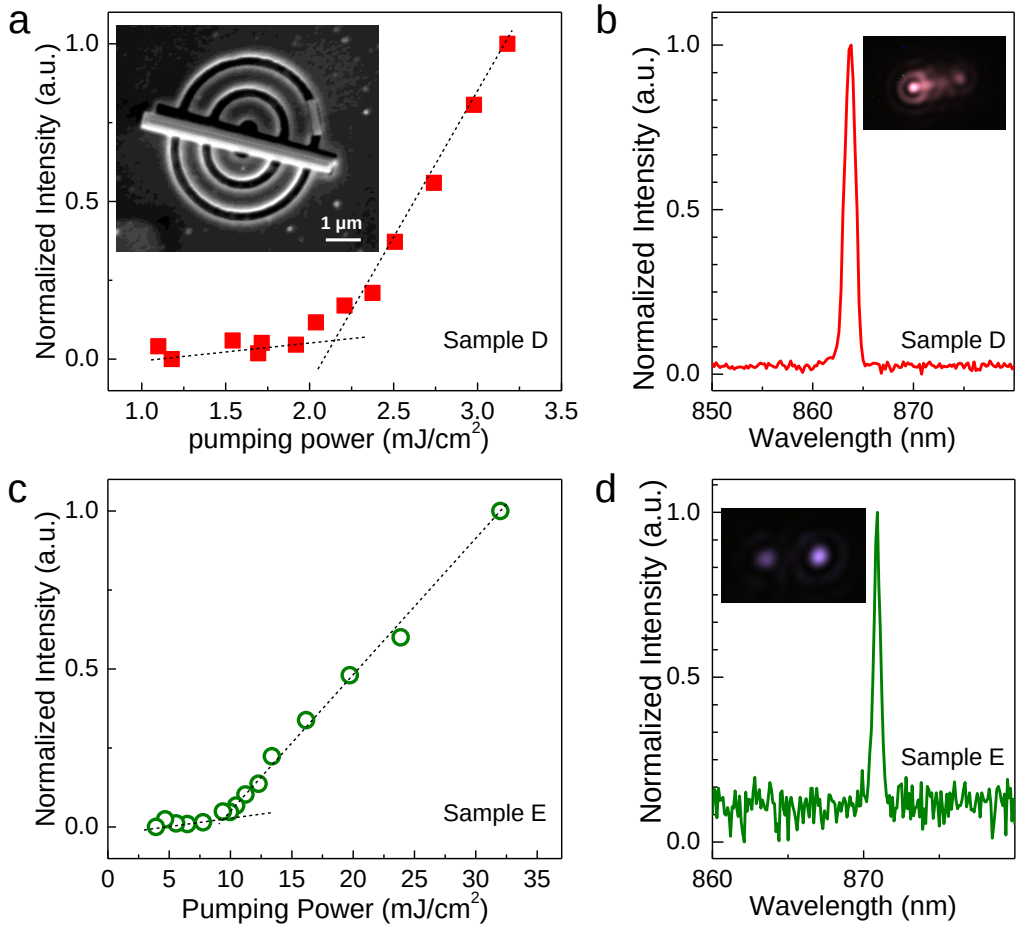

Figure 4. Room-temperature lasing characterization of Samples D and E (nanowires with larger dimensions). (a) Lasing threshold curve for Sample D, showing a lasing threshold of ~2 mJ/cm^2. The inset shows the SEM image of Sample D with a single InP NW laser (w = 435 nm, L = 5 µm) printed onto a CE antenna. (b) Spectral emission of Sample D obtained at the fluence of 4.68 mJ/cm^2. The inset shows an optical micrograph of the NW lasing. (c) Threshold curve of the bare NW laser (Sample E) with a threshold of ~10 mJ/cm^2. (d) Emission spectrum of Sample E at a fluence of 32.01 mJ/cm^2. The inset shows the optical micrograph of the lasing at the same pump intensity.

In summary, we report a novel design capable of tailoring and enhancing the light emission properties of ultra-small-size InP nanowire (NW) lasers. By integrating an InP NW with an *Al* cat's eye (CE) nanoantenna we demonstrate lasing and vertical emission with enhanced performance from InP NWs with very small dimensions (w = 290 nm, L = 900 nm) at low temperatures. Also, using larger InP NWs (w = 435 nm, L = 5 µm) in the NW-CE antenna configuration, we demonstrate room temperature lasing with reduced lasing threshold. Moreover, we reveal that this InP NW CE laser design provides a highly-

improved light emission performance in multiple ways including: (i) enhanced directionality/focused far-field distribution, attributed to the presence of surface waves and their constructive interference with the emitted light; (ii) a higher degree of polarization (DOP), arising from the cylindrical symmetry breaking in the CE's nanoantenna structure; (iii) increased internal quantum efficiency and reduced pumping power requirements for the onset of lasing operation, as a result of Purcell enhancement. Furthermore, we report two fabrication approaches for the InP NW CE lasers using either direct patterning or a hybrid nanoscale Transfer Printing technique to precisely place the NW onto a pre-fabricated CE antenna. Finally, this InP NW CE laser design could also be applicable to other types of semiconductor NWs based on different material systems and structural composition, thus offering excellent promise for the development of nanoscopic light sources with dramatically-enhanced performance for use in future integrated nanophotonics systems and applications.

Methods. *Nanowire (NW) growth.* As described in our previous work [8], the InP NWs were grown on (111)A InP substrates by selective area epitaxy (SAE). The SEM images of the top section and tilted views included in Supporting Information (Figure S5) show that the NWs have excellent uniformity. The average width of the NWs (i.e., the diameter), *w*, was 290 nm. After transferring the NWs onto a quartz substrate, the average length, *L*, was measured to be 900 nm. Similar growth processes have been used to fabricate the larger and longer nanowires (w = 435 nm, L = 5 μm) used in the RT lasing experiments. The main difference lies in the hole pitch and size in the SiO_2 mask layer [8].

Device fabrication. (i) Fabrication for Sample A (w = 290 nm, L = 900 nm) began by first transferring the NWs from the growth substrate onto a quartz substrate. Then a layer of 300 nm-thick SiO_2 was deposited by plasma enhanced chemical vapor deposition (PECVD), followed by a 30 nm *Al* deposition via e-beam evaporation. The *Al* layer also functioned as the conducting layer in the following focused ion beam (FIB) etching steps. For the FIB etching process, a NW was firstly located in the middle of SEM view field, with its axial direction aligned to the *y*-axis. The antenna design was then imported by intaglio

printing into the *SiO_2/Al* structure around the InP NW with depth of ~330 nm, as can be seen in Figure 1e. Finally, another 1 μm-thick *Al* layer was deposited to form the CE antenna. Given that the FIB system has very small system error in alignment, ~0.1° in angle and 20 nm in-plane, near ideal alignment could be obtained between the antenna pattern and the InP NW even with ultra-small geometries. This *in-situ* fabrication method is therefore very promising for future hybrid NW-nanoantenna constructions. (ii) A nanoscale Transfer-Printing (nano-TP) technique was used for the fabrication of Samples D and E with relatively larger InP NWs (w = 435 nm, L = 5 μm). First, the *Al* antenna was produced on a quartz substrate with standard e-beam evaporation for metal layer and FIB etching for the patterning of the CE antenna. After this, using a bespoke polydimethyl sulfoxide (PDMS) μ-stamp, an individual InP NW was 'captured' from a carrying substrate (*Si*) and printed on the central gap of the fabricated CE nanoantenna. For full details on this nano-TP technique see [26,27].

Optical measurements. (i) Samples A, B and C (w = 290 nm, L = 900 nm) were optically excited using a Yb:YAG laser with a pulse duration of 300 fs and 20.8 MHz repetition rate, frequency-doubled to a wavelength of 522 nm using an LBO crystal. The laser beam was focused through a 60x microscope objective lens, resulting in a spot size of ~ 0.5 μm as estimated by vector diffraction calculation. The emission was collected by the same objective lens and detected by a single photon avalanche diode, which was connected to a Picoharp 300 time-correlated single photon counting (TCSPC) system. (ii) Samples D and E (w = 435 nm, L = 5 μm) were optically measured at room temperature using a 532 nm frequency-doubled Nd:YAG pulsed laser with a pulse width of 1.6 ns and a repetition rate of 10 kHz. Full details on the setup used to characterize Samples D and E are given in [26,27].

ASSOCIATED CONTENT

Supporting Information

Additional information on the design of the InP nanowires (NWs) and cat's eye (CE) antennas, threshold gain modeling, growth of InP nanowires, hybrid fabrication of room temperature InP NW CE lasers, and

room temperature radiation patterns of InP NW CE lasers. The Supporting Information is available free of charge on the ACS Publications website at DOI: 10.1021/acs.nanolett. XXXXXXX.

AUTHOR INFORMATION

Corresponding Authors

∗e-mail: ffren@nju.edu.cn; antonio.hurtado@strath.ac.uk

Author contributions

F.-F. R. and C. J. proposed the device to realize nanowire lasing with high directionality, high efficiency and high degree of polarization. W.-Z. X., F.-F. R., and L. L. proposed the FIB based *in-situ* antenna patterning method. D. J., B. G., A. H. and M. D. developed the nanoscale Transfer-Printing (nano-TP) technique. Q. G., H. H. T. and L. F. optimized the growth conditions for the nanowires. W.-Z. X., L. L. and D. J. fabricated samples, W.-Z. X., D. J., J. Y., and F. W. performed the measurements, F.-F. R. completed numerical simulations, W.-Z. X., F.-F. R., D. J., J. Y., A. H., B. G., L. F., H. H. T., M. D. and C. J. discussed the comparisons between simulations and experiments, H. L., R. Z., H. H. T., A. H. M. D. and C. J. coordinated the study. All the authors discussed the results and contributed to the writing of manuscript. †These authors contributed equally.

Notes

The authors declare no competing financial interest.

ACKNOWLEDGMENTS

This work was supported by the National Key R&D Program of China (No. 2016YFB0400105), the Australian Research Council, the National Natural Science Foundation of China (No. 61774081), the Natural Science Foundation of Jiangsu Province, China (No. BK20161401), the Fundamental Research

Funds for the Central Universities under Grant No. 021014380071, and the UK EPSRC Doctoral Training Partnership. Access to epitaxy and device fabrication facilities used in this work was made possible through the Australian National Fabrication Facility, ACT Node.

REFERENCES

(1). Yang, P.; Yan, R.; Fardy, M. *Nano Lett.* **2010**, *10* (5), 1529-1536.

(2). Yan, R.; Gargas, D.; Yang, P. *Nat. Photon.* **2009**, *3* (10), 569-576.

(3). Saxena, D.; Mokkapati, S.; Parkinson, P.; Jiang, N.; Gao, Q.; Tan, H. H.; Jagadish, C. *Nat. Photon.* **2013**, *7* (12), 963-968.

(4). Claudon, J.; Bleuse, J.; Malik, N. S.; Bazin, M.; Jaffrennou, P.; Gregersen, N.; Sauvan, C.; Lalanne, P.; Gérard, J. M. *Nat. Photon.* **2010**, *4* (3), 174-177.

(5). Hochbaum, A. I.; Yang, P. *Chem. Rev.* **2009**, *110* (1), 527-546.

(6). Krogstrup, P.; Jørgensen, H. I.; Heiss, M.; Demichel, O.; Holm, J. V.; Aagesen, M.; Nygard, J.; i Morral, A. F. *Nat. Photon.* **2013**, *7* (4), 306-310.

(7). Zhu, H.; Fu, Y.; Meng, F.; Wu, X.; Gong, Z.; Ding, Q.; Gustafsson, M. V.; Trinh, M. T.; Jin, S.; Zhu, X. Y. *Nat. Mater.* **2015**, *14* (6), 636.

(8). Gao, Q.; Saxena, D.; Wang, F.; Fu, L.; Mokkapati, S.; Guo, Y.; Li, L.; Wong-Leung, J; Caroff, P.; Tan, H. H.; Jagadish, C. *Nano Lett.* **2014**, *14* (9), 5206-5211.

(9). Johnson, J. C.; Choi, H. J.; Knutsen, K. P.; Schaller, R. D.; Yang, P.; Saykally, R. J. *Nat. Mater.* **2002**, *1* (2), 106-110.

(10). Oulton, R. F. *et al*. Oulton, R. F.; Sorger, V. J.; Zentgraf, T.; Ma, R. M.; Gladden, C.; Dai, L.; Bartal, G.; Zhang, X. *Nature* **2009**, *461* (7264), 629-632.

(11). Vanmaekelbergh, D.; Van Vugt, L. K. *Nanoscale* **2011**, *3* (7), 2783-2800.

(12). Grzela, G.; Paniagua-Domínguez, R.; Barten, T.; Fontana, Y.; Sánchez-Gil, J. A.; Gómez Rivas, J. Nanowire antenna emission. *Nano Lett.* **2012**, *12* (11), 5481-5486.

(13). Saxena, D.; Wang, F.; Gao, Q.; Mokkapati, S.; Tan, H. H.; Jagadish, C. Mode Profiling of semiconductor nanowire lasers. *Nano Lett.* **2015**, *15* (8), 5342-5348.

(14). Sorger, V. J.; Zhang, X. *Science* **2011**, *333* (6043), 709-710.

(15). Noginov, M. A.; Zhu, G.; Belgrave, A. M.; Bakker, R.; Shalaev, V. M.; Narimanov, E. E.; Stout, S.; Herz, E.; Suteewong, T.; Wiesner, U. Demonstration of a spaser-based nanolaser. *Nature* **2009**, *460* (7259), 1110-1113.

(16). Gramotnev, D. K.; Bozhevolnyi, S. I. *Nat. Photon.* **2010**, *4* (2), 83-91.

(17). Ma, R. M.; Oulton, R. F.; Sorger, V. J.; Bartal, G.; Zhang, X. *Nat. Mater.* **2011**, *10* (2), 110-113.

(18). Lu, Y. J.; Kim, J.; Chen, H. Y.; Wu, C.; Dabidian, N.; Sanders, C. E.; Wang, C. Y.; Lu, M. Y.; Li, B. H.; Qiu, X.; Chang, W. H.; Chen, L. J.; Shvets, G.; Shih, C. K.; Gwo, S. Plasmonic nanolaser using epitaxially grown silver film. *Science* **2012**, *337* (6039), 450-453.

(19). Khajavikhan, M.; Simic, A.; Katz, M.; Lee, J. H.; Slutsky, B.; Mizrahi, A.; Lomakin, V.; Fainman, Y. Thresholdless nanoscale coaxial lasers. *Nature* **2012**, *482* (7384), 204-207.

(20). Ren, F. F.; Ang, K. W.; Ye, J.; Yu, M.; Lo, G. Q.; Kwong, D. L. Split bull's eye shaped aluminum antenna for plasmon-enhanced nanometer scale germanium photodetector. *Nano Lett.* **2011**, *11* (3), 1289-1293.

(21). Rosenwaks, Y.; Shapira, Y.; Huppert, D. *Appl. Phys. Lett.* **1990**, *57* (24), 2552-2554.

(22). Yang, M.; Ren, F. F.; Pu, L.; Xiao, L.; Sheng, Y.; Wang, J.; Zheng, Y.; Shi, Y. Split bull's eye antenna for high-speed photodetector in the range of visible to mid-infrared. *IEEE Photon. Technol. Lett.* **2016**, *28* (11), 1177-1180.

(23). Beruete, M.; Campillo, I.; Dolado, J. S.; Rodríguez-Seco, J. E.; Perea, E.; Falcone, F.; Sorolla, M. Very low-profile "Bull's Eye" feeder antenna. *IEEE Antennas and Wirel. Propag. Lett.* **2005**, *4* (1), 365-368.

(24). Rivera, V. A. G.; Ferri, F. A.; Nunes, L. A. O.; Zanatta, A. R.; Marega Jr., E. *Appl. Phys. A* **2012**, *109* (4), 1037-1041.

(25). Fattal, D.; Li, J.; Peng, Z.; Fiorentino, M.; Beausoleil, G. R. *Nat. Photon.* **2010**, *4* (7), 466-470.

(26). Guilhabert, B.; Hurtado, A.; Jevtics, D.; Gao, Q.; Tan, H. H.; Jagadish, C.; Dawson, M. D. Transfer printing of semiconductor nanowires with lasing emission for controllable nanophotonic device fabrication. *ACS Nano* **2016**, *10* (4), 3951-3958.

(27). Jevtics, D.; Hurtado, A.; Guilhabert, B.; McPhillimy, J.; Cantarella, G.; Gao, Q.; Tan, H. H.; Jagadish, C.; Strain, M. J.; Dawson, M. D. Integration of semiconductor nanowire lasers with polymeric waveguide devices on a mechanically flexible substrate. *Nano Lett.* **2017**, *17* (10), 5990-5994.

(28). Rau, B.; Waltereit, P.; Brandt, O.; Ramsteiner, M.; Ploog, K. H.; Puls, J.; Henneberger, F.; In-plane polarization anisotropy of the spontaneous emission of M-plane GaN/(Al, Ga) N quantum wells. *Appl. Phys. Lett.* **2002**, *77* (21), 3343-3345.

(29). Sun, Y. J.; Brandt, O.; Ramsteiner, M.; Grahn, H. T.; Ploog, K. H. *Appl. Phys. Lett.* **2003**, *82* (22), 3850-3852.

(30). Wang, F.; Gao, Q.; Peng, K.; Li, Z.; Li, Z.; Guo, Y.; Fu, L.; Smith, L. M.; Tan, H. H.; Jagadish, C. Spatially resolved doping concentration and nonradiative lifetime profiles in single Si-doped InP nanowires using photoluminescence mapping. *Nano lett.* **2015**, *15* (5), 3017-3023.